ADVANCED MATERIALS

www.advmat.de

An Autotransferable g-C_3N_4 Li^+-Modulating Layer toward Stable Lithium Anodes

Yanpeng Guo, Ping Niu, Yayuan Liu, Yan Ouyang, Dian Li, Tianyou Zhai, Huiqiao Li, and Yi Cui**

Commercial deployment of lithium anodes has been severely impeded by the poor battery safety, unsatisfying cycling lifespan, and efficiency. Recently, building artificial interfacial layers over a lithium anode was regarded as an effective strategy to stabilize the electrode. However, the fabrications reported so far have mostly been conducted directly upon lithium foil, often requiring stringent reaction conditions with indispensable inert environment protection and highly specialized reagents due to the high reactivity of metallic lithium. Besides, the uneven lithium-ion flux across the lithium surface should be more powerfully tailored via mighty interfacial layer materials. Herein, g-C_3N_4 is employed as a Li^+-modulating material and a brand-new autotransferable strategy to fabricate this interfacial layer for Li anodes without any inert atmosphere protection and limitation of chemical regents is developed. The g-C_3N_4 film is filtrated on the separator in air using a common alcohol solution and then perfectly autotransferred to the lithium surface by electrolyte wetting during normal cell assembly. The abundant nitrogen species within g-C_3N_4 nanosheets can form transient Li—N bonds to powerfully stabilize the lithium-ion flux and thus enable a CE over 99% for 900 cycles and smooth deposition at high current densities and capacities, surpassing most previous works.

Lithium-metal batteries (LMBs) such as lithium–air and lithium–sulfur batteries have ignited extensive research interests for their high energy density.[1–3] However, the commercial deployment of lithium (Li) metal anode has been severely impeded by problems such as poor battery safety, unsatisfying cycling lifespan and efficiency.[4] Previous reports confirmed that the uneven ion distribution in the vicinity of the anode can trigger nonuniform Li deposition morphology (often referred to as "dendrite"), which may further induce internal short circuits.[5–8] Besides, the high (electro)chemical reactivity of metallic Li toward electrolyte species leads to continuous consumption of electrolytes, resulting in poor lifespan with low Coulombic efficiency.[9]

Recently, building external interfacial layers over Li anode has been regarded as an effective strategy.[10–13] Different materials, such as flexible organic polymers (poly(dimethylsiloxane) (PDMS), poly(vinylidene fluoride) (PVDF), poly(vinylidene fluoride-*co*-hexafluoropropylene) (PVDF-HFP), etc.) and rigid inorganics (LiF, Li_3N, Li_3PO_4, etc.), were adopted to suppress dendrite growth or block the direct reaction between Li and electrolyte.[14,15] With these interfacial protective layers, the cycling lifespan of Li anode can be extended from tens of cycles to a level of several hundred cycles. However, it remains challenging to surpass 500 cycles for the present interfacial layers in a Li–Cu half cells. One possible reason is that most previous interfacial layers are generally designed from the mechanical view to suppress dendrite. In fact, the more significant thing is to tune the interaction between Li ion and coating materials to enable uniform ion flux at the interfacial, which refers to the chemical-based means through rational materials selection. For example, materials such as doped graphene, polydopamine, oxidized PAN nanofiber, etc., are reported capable to form strong interactions toward Li ions via polar functional groups and hence contribute to homogenize the Li^+ flux.[16–19] Moreover, another big challenge for the current interfacial layers is that they were mostly built straight upon Li foil via solution coating or physical sputtering.[14,20] Due to the unparalleled reactivity of metallic Li, all the procedures have to be conducted in vacuum or inert atmospheres, giving rise to high fabrication cost and harsh operation conditions. Meanwhile, all the involving chemical regents during the operation should be paid special attentions to avoid undesirable side reactions with metallic Li, which greatly limits the possible choices of interfacial materials.[21] Therefore, smart techniques devoid of aforementioned demerits to establish protective layers are highly desired.

Here, we develop a brand-new autotransferable strategy to fabricate an interfacial layer for Li metal by employing graphene-like carbon nitride (GCN, g-C_3N_4) (**Figure 1**). While writing this manuscript, we notice that there is one publication

Y. Guo, P. Niu, Y. Ouyang, D. Li, Prof. T. Zhai, Prof. H. Li
State Key Laboratory of Material Processing and Die and Mould Technology
School of Materials Science and Engineering
Huazhong University of Science and Technology
Wuhan 430074, P. R. China
E-mail: hqli@hust.edu.cn
Dr. Y. Liu, Prof. Y. Cui
Department of Materials Science and Engineering
Stanford University
Stanford, CA 94305, USA
E-mail: yicui@stanford.edu

The ORCID identification number(s) for the author(s) of this article can be found under https://doi.org/10.1002/adma.201900342.

DOI: 10.1002/adma.201900342

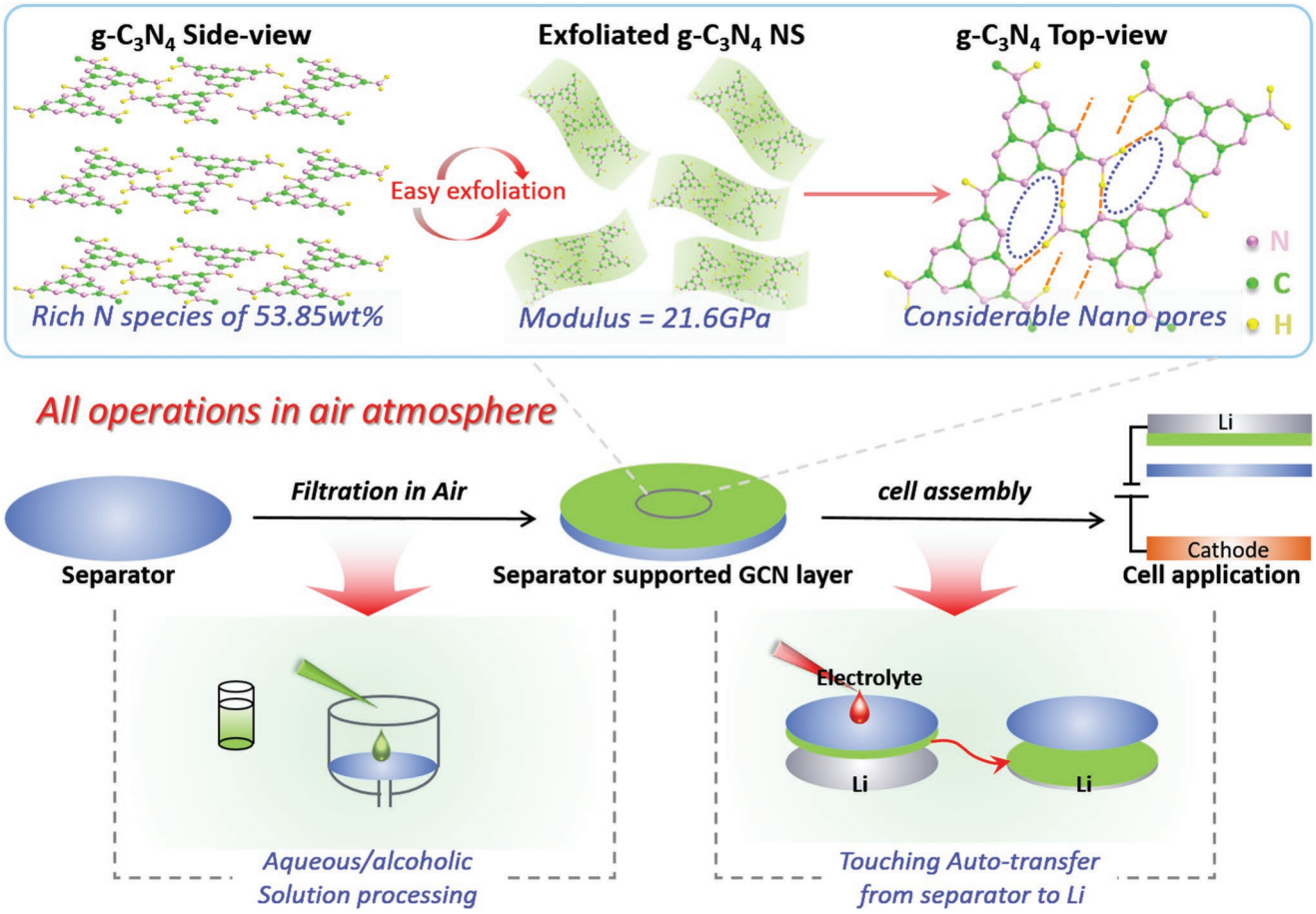

Figure 1. Structure, properties, and schematic illustration of construction of interfacial g-C_3N_4 Li^+-modulating layer using as-proposed touching autotransfer tactic.

just coming out about using g-C_3N_4 as surface modification materials for Ni foam 3D host to adjust the microelectric field and guide Li deposition.[22] In our work, the g-C_3N_4 is used in the form of an integrated film and functions as a continuous Li^+-modulating layer at the electrode/electrolyte interface via the formation of Li—N bonds. The predominating N species within g-C_3N_4 up to 53.85 wt%, which is hardly observed in other materials, could provide considerable amount of adhesive sites to interact with Li ions. Besides, g-C_3N_4 holds a typical layered structure in which the weak van der Waals force between layers ensures the easy exfoliation into few-layered nanosheets to expose more surface sites, while the strong covalent in-plane interaction contributes to the integrity of individual layers and an ultrahigh shear modulus up to ≈21.6 GPa to help resist dendrite proliferation upon cycling.[23–25] The g-C_3N_4 Li^+-modulating layer was successfully built through a simple two-step approach by first vacuum filtrating the g-C_3N_4 suspension into a thin film over the separator in ambient air and then autotransfer the film to Li anode surface merely by electrolyte wetting during the normal cell assembly process. Such technique avoids the direct operation upon Li and thus requires no special protection and shows little limitation in chemical reagents. Various low-price solvents which are generally believed incompatible with metallic Li such as water, ethanol, etc., are now becoming usable to replace the expensive, poisonous, and extra-dry Li-inert solvents such as tetrahydrofuran. In the presence of such a g-C_3N_4 interfacial layer, the abundant N species are confirmed able to form transient Li—N bonds to powerfully homogenize the Li^+ distribution at the vicinity of anode surface, and lower the nucleation overpotential via reducing the energy consumed upon Li desolvation. And the ion transport process is also promoted by the innately rich structural defects and nanopores in g-C_3N_4. Therefore, Li anode equipped with such g-C_3N_4 Li^+-modulating layer can be effectively stabilized with a CE over 99% for 900 cycles with smooth deposition at high current densities and capacities, surpassing most previous works.

Bulk C_3N_4 powder are synthesized via the polycondensation of urea with properties presented in Figure S1 (Supporting Information). A homogenous g-C_3N_4 nanosheets dispersion is then prepared by ultrasonic exfoliation of the bulk powder, which remains stable after months of rest and is ready for use in the following vacuum filtration (**Figure 2**a). The as-prepared g-C_3N_4 nanosheets are several microns in length and 2–4 nm in thickness, with a laminar morphology like silk veil similar to graphene as depicted in atomic force microscopy (AFM) and transmission electron microscopy (TEM) images (Figure 2b,c). Such morphology of g-C_3N_4 nanosheets enable their face-to-face self-assembly into a freestanding film via facile vacuum

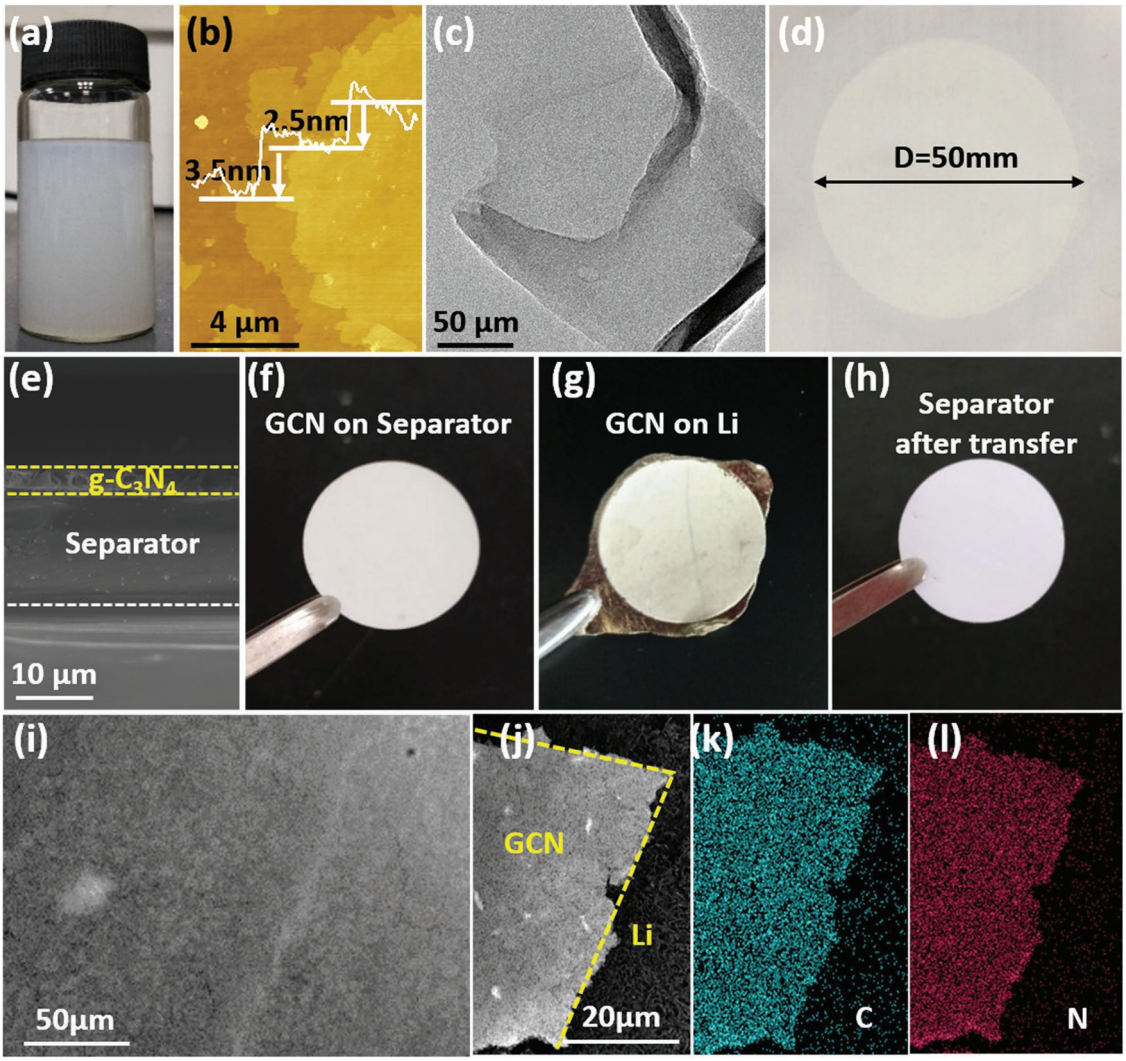

Figure 2. a) g-C_3N_4 (GCN) dispersions after 10 h sonication in isopropyl alcohol followed by centrifugation. b) Tapping-mode AFM image of a single GCN nanosheet deposited on the silicon wafer substrate. c) TEM images of exfoliated GCN nanosheets. d) Photograph and e) side-view SEM images of separator coved with GCN nanosheets via vacuum filtration. f–h) Photographs of GCN over the separator (f), GCN on Li after transfer merely using electrolyte wetting (g), and separator after transfer (h). i) Top-view SEM images of GCN over a lithium anode. j) A typical SEM image at the boundary of GCN-modified and unmodified lithium surface, and k,l) corresponding C (k) and N (l) EDS elemental mapping.

filtration. Additional nanopores stemming from the breakage of hydrogen bonds could be observed, allowing easy transport of Li ion across the interface layer.[26] A few-micrometer-thick g-C_3N_4 film of 50 mm in diameter was prepared in ambient air using the commercial Celgard separator as the filter membrane (Figure 2d,e) indicating the great potential of the technique toward large-scale preparation. Afterward, this GCN-covered separator was assembled into LMBs with GCN facing to the Li anode. Figure 2f–h shows the photographs of GCN-covered separator, GCN-covered Li, and the separator after transfer respectively. The faint yellow–colored GCN film could be entirely and automatically transferred to the anode surface and remains intact, which are further confirmed by scanning electron microscopy (SEM) images in Figure 2i. The energy-dispersive X-ray spectroscopy (EDS) elemental mapping over the Li surface with or without a GCN film shows a clear boundary (Figure 2i–l). Besides, C and N signals coming from the GCN protective layer are uniformly distributed, confirming its well-preserved integrity. g-C_3N_4 films with different thickness were prepared by changing the volume of the dispersion upon the initial vacuum filtration process. The table in Figure S2 (Supporting Information) lists the thickness of varied films measured by micrometer. Figure S2a–f (Supporting Information) demonstrates the photographs of Li foil after autotransfer. All films well maintained its original integrity after autotransfer, implying that the process shows good tolerance upon thickness from several micrometer to tens of micrometer. Besides, this autotransfer technique shows good universality and could be expanded into materials that possess superior lithiophilicity or strong interactions toward Li. More examples including acid-treated CNT, graphene oxide, and vanadium oxide were also tried to serve such interfacial layer and all of them are well autotransferrable via this tactic in Figure S3 (Supporting Information).

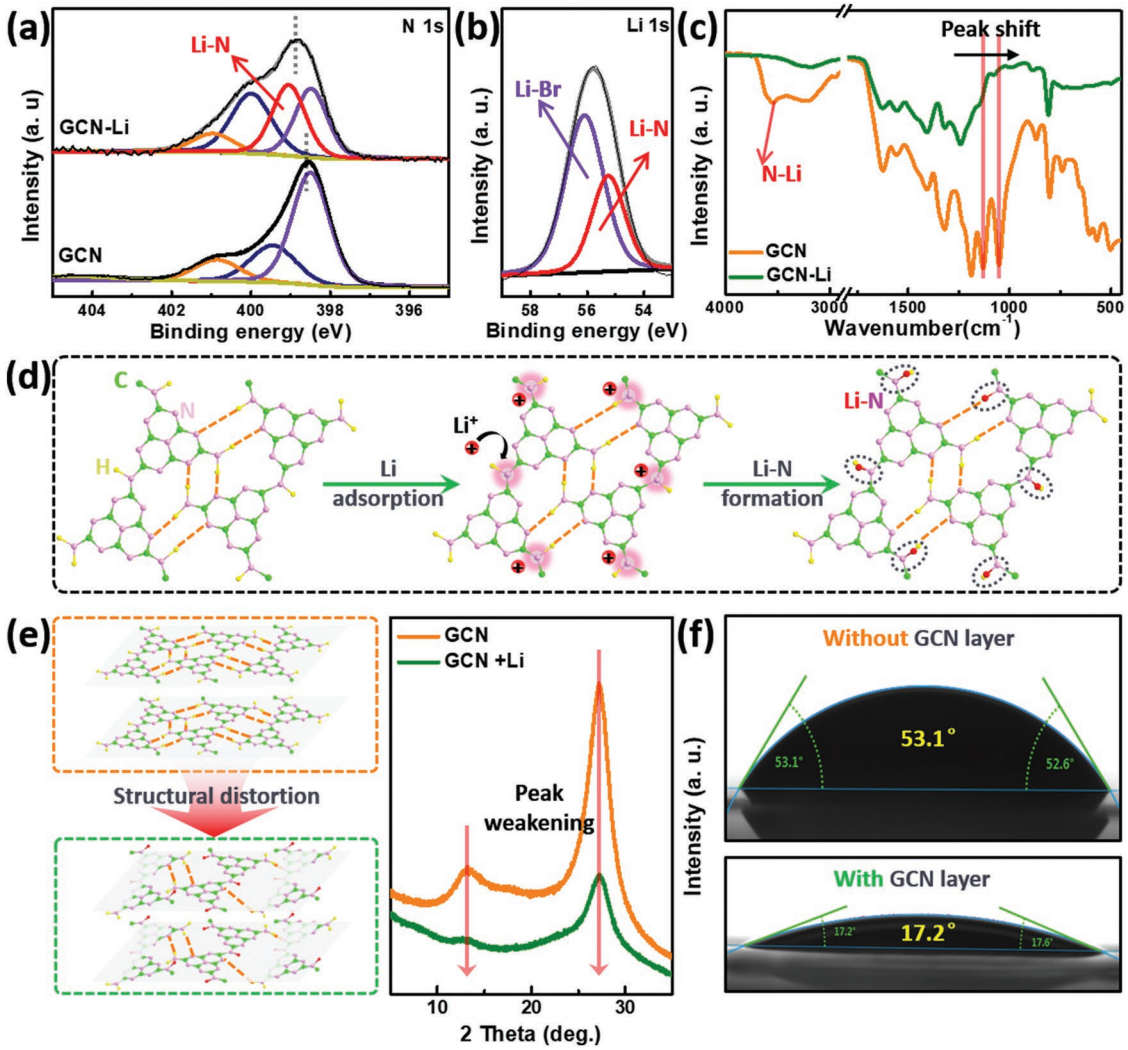

Figure 3. a) N 1s XPS spectra, b) Li 1s XPS spectra, and c) FTIR spectra of GCN nanosheet before and after Li-salt solution treatment. d) Schematic illustration of transient Li—N bonds formation over the GCN nanosheets. e) XRD patterns of g-C_3N_4 nanosheet before and after Li-salt solution treatment. f) Contact angles of electrolyte toward anode without and with a GCN layer.

The GCN are deliberately chosen for its abundant N species which are reported able to interact with Li ions.[19] The lone pair electrons of the N-species within GCN interfacial layer are expected to act as Lewis base sites to strongly attract Lewis acidic Li ions in electrolytes through acid–base interactions, promising the capability to modulate the ion concentration over the anode surface. To confirm the above assumption, a GCN layer is immersed in a Li-salt solution for 1 h, washed and dried overnight. Lithium bromide (LiBr) was adopted as Li salt to eliminate the influence of innate N species in the electrolyte salt (LiTFSI). X-ray photoelectron spectroscopy (XPS) was then performed to investigate the chemical state of nitrogen within the GCN layer to characterize its interactions toward Li ions. The N 1s spectra of g-C_3N_4 nanosheet before Li-salt treatment could be deconvoluted into three major peaks located at 400.8, 399.5, and 398.5 eV, which belong to N—H bonds, bridging N atoms in N—$(C)_3$, and sp^2 N atoms involved in triazine rings, respectively.[27] After Li-salt solution treatment, an additional peak at 398.7 eV emerged, which was ascribed to the newly formed Li–N peak according to XPS data for pristine Li_3N (**Figure 3**a; Figure S4, Supporting Information). The blueshift of N1s revealed that Li ions probably shared the lone-pair electrons of N atoms and thus decreased the probability density distribution at the vicinity of nitrogen atoms. The Li 1s spectra can be as well divided into two peaks including Li atoms coming from Li—Br bonds at 56.8 eV that originated from residual LiBr compounds and Li—N bonds at 55.2 eV (Figure 3b; Table S1, Supporting Information). Fourier transform infrared (FTIR) spectroscopy was performed to further investigate the structural changes within GCN structures after Li-salt treatment. Changes can be detected as shown in Figure 3c, peak shifts in the region 900–1800 cm^{-1} happens due to the introduction of alien Li ions that disrupt the original bond vibrations. Another remarkable change located at the stretch mode of N—H bonds shows an obvious peak splitting as a result of the formation of additional Li—N bonds. Based upon these results, we assume that those negatively charged N atoms with dangling lone-pair electrons could attract plenty

of positively charged Li ions around and facilitate the desolvation of Li ions, ending up with the formation of transient Li—N bonds. The distribution of Li ions is greatly depended on the distribution of N species. Given the as-prepared stable and uniform g-C_3N_4 layer, the Li ion distribution is thus significantly homogenized and the movement of Li ions toward the "hot spots" is retarded by the attraction force from N species during Li plating (Figure 3d). The crystal and chemical structure of the GCN nanosheets before and after Li-salt immersion were further analyzed by X-ray diffraction (XRD). Two typical diffraction peaks centered at 13.1° and 27.2° represents the intralayer long-range atomic order and interlayer periodic stacking along the *c*-axis in graphitic carbon nitride, respectively.[28] The weakening and widening of these two peaks after Li-salt immersion indicate the breaking of periodic stacking and structural order owing to the introduction of Li ions. Afterward, the electrolyte wettability toward the GCN layer is as well measured to explore the effect of such a layer on the interfacial physical properties (Figure 3f). Results show that the presence of the GCN layer greatly enhanced the electrolyte wettability with a much decreased contact angle from 53.1° to 17.2°. The electrolyte wettability has a close relationship with the uptake amount of liquid electrolyte and then affects the distribution of Li ion flux over the entire Li surface during cycling.[18] And such a superior electrolyte wettability toward the GCN layer is conducive to the uniformity of Li ion flux to mitigate uneven Li ion transport and deposition.

To investigate GCN's effect on the electrode kinetics, Li–Cu half cells or Li–Li symmetric cells were assembled for measurements. First, the nucleation overpotential at the beginning of deposition is probed.[19,29] The overpotential values with or without a GCN layer were calculated to be 48.3 and 109.5 mV, respectively, reflecting that the GCN layer significantly lowered that Li deposition barrier (**Figure 4**a). The reason could be ascribed to the accelerated desolvation process at the anode–electrolyte interface. Before deposition, Li ions are directly connected to the g-C_3N_4 nanosheets due to the strong chemical interactions instead of intensely solvated by solvent molecules and thus speed up the dissociation of Li ions and lithium salt. Besides, the higher Li^+ flux at the interface due to prebonding by the GCN layer increases the reactant concentration and promotes the deposition step ($Li^+ + e^- = Li$) as well. The activation energy for Li deposition was also measured via temperature-dependent electrochemical impedance spectroscopy (EIS) tests (Figure 4b). The EIS characterization was taken under different temperatures from 278 to 303 K as shown in Figure S5 (Supporting Information). Data obtained from both cases were well fitted to straight lines using the Arrhenius equation:

$$\frac{T}{R_{ct}} = A \exp\left(-\frac{E_a}{RT}\right) \tag{1}$$

where E_a is the activation energy, T is the absolute temperature, R is the gas constant, R_{ct} is the interfacial lithium-ion transfer resistance, and A is the pre-exponential factor.[30,31] The activation energy upon deposition were valued at 6.766 and 11.118 kJ mol^{-1}, respectively, with or without a GCN layer, which further confirms the active role GCN played upon Li deposition. The exchange current density was also measured using Equation (2)

$$i \approx i_0 \frac{F}{RT} \frac{\eta_{tot}}{2} \tag{2}$$

where η_{tot} is the total overpotential. Two-electrode symmetric cells were assembled followed by galvanostatic cycling at various currents from 5 to 120 μA to explore the effect of a GCN layer on the interfacial kinetics (Figure 4c; Figure S6, Supporting Information).[32] Pristine cell presents a low exchange current density of 0.482 mA, indicating its rather sluggish deposition kinetics. With the help of a GCN layer, the exchange current density rises to 0.866 mA owing to a prestabilized Li^+ distribution that provides adequate Li ions for deposition and thus facilitate the kinetics at the vicinity of the anode. Cyclic voltammetry was as well performed in a Li–Cu half-cell at various rates (Figure 4d; Figure S7, Supporting Information). The pronounced redox peaks varies with increasing sweep rates (v) during voltammetry experiments and the relation is expressed as $i = av^b$ with the value of b providing insight on the charge storage mechanism.[33] Generally, a b-value of 0.5 would indicate that the current is controlled by semi-infinite linear diffusion and a value of 1 indicates that the current is surface controlled.[34] Data from CV curves were well fitted into a straight lines to extact b-values using this equation. In the presence of a GCN layer, a huge increase in b from 0.338 to 0.609. The results revealed that the pristine diffusion-limited process might be partially transformed into a surface-controlled one with the help of a GCN layer, indicating an adequate Li ion source in close proximity to lithium surface upon plating/stripping. To sum up as shown in Figure 4e,f, the deposition of Li ions could be generally divided into three steps: the ion diffusion within the electrolyte, the ion desolvation at the Li–electrolyte interface and the Li plating over the Li surface. As a rule, the desolvation process at the interface could be the rate-determining step and its large energy barrier needs to be conquered. Assisted by the GCN interfacial layer, amounts of Li ions tends to desolvate in advance to form transient Li—N bonds before deposition and thus leads to a much smaller energy barrier for deposition.

The impact of GCN on morphology evolutions were monitored by SEM as depicted in **Figure 5**. Li deposition on the bare Cu foil exhibits mossy and dendrite structures at a current density of 1 mA cm^{-2} after ten cycles and then evolved into large loosely connected Li particles at the end of 100 cycles. Such structural characterizations are tightly related to the unstrained dendrite growth and sequential dead Li formation, leading to the continuous consumption of active Li source and electrolytes. Upon prolonged cycling to 200 cycles, the morphology gets more porous with numerous pores that cut down the electron pathways within the anode, leading to cell "dry-out" or safety risks (Figure 5a). On the contrary, Li–Cu cells equipped with Li^+ modulating layer demonstrate a smooth deposition without any dendrites. Deposited Li particles were tightly connected, implying unhindered electron pathways for fast charge transfer (Figure 5b). Corresponding top-view elemental mapping images after 200 cycles are presented in Figure S8 (Supporting Information). Compared to bare anode which majorly possess C and O species, the surface of the Li-deposited Cu disassembled from Li–GCN–Cu cells are covered by C and N species coming from GCN. Generally, Li ions are solvated with

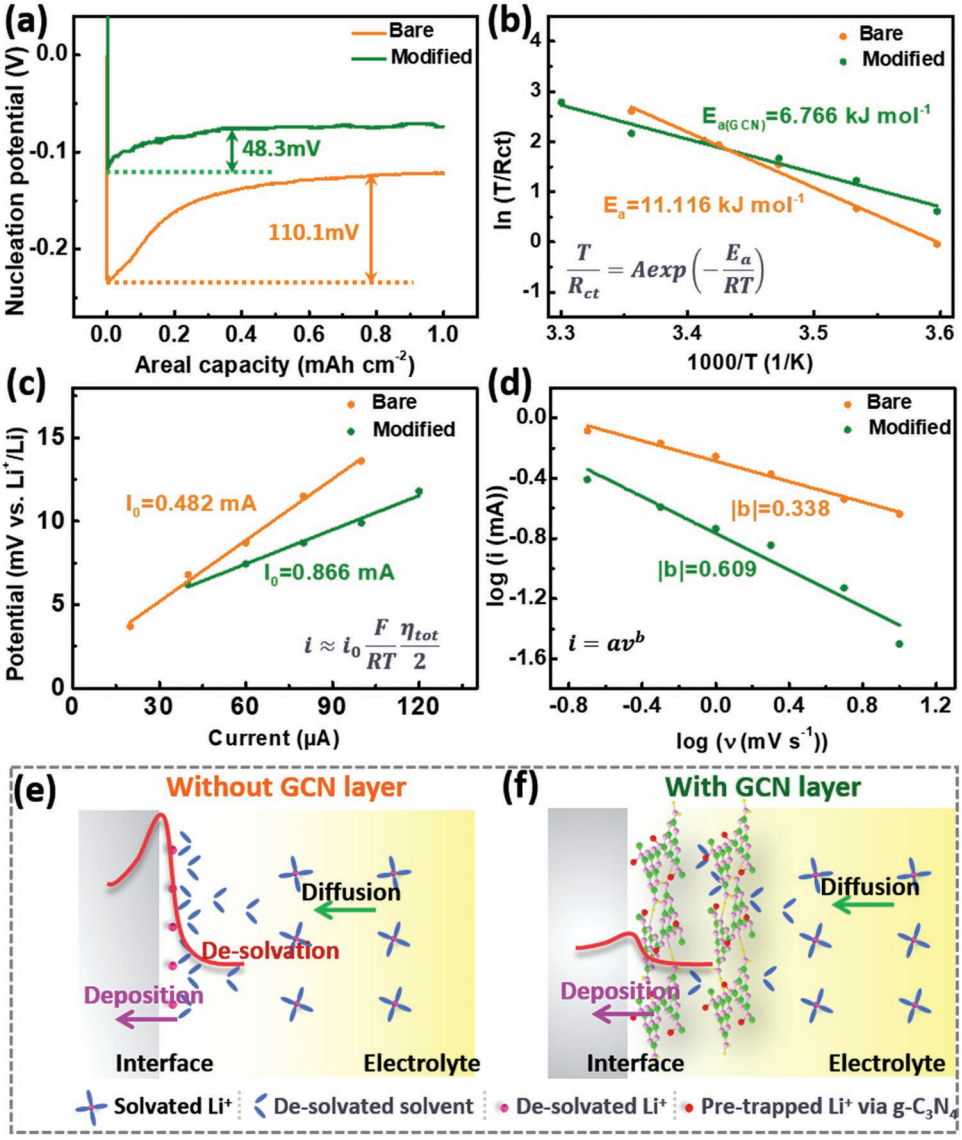

Figure 4. a) Nucleation overpotential and b) apparent activation energy required in cells with bare anode and GCN Li^+-modulating layer modified anode. It can be observed that the presence of GCN Li^+-modulating layer significantly lowered the energy barrier for deposition which would further benefit a smooth and uniform deposition morphology over the anode surface. c) Exchange current density and d) linear fitting of lg(oxidative peak current) to lg(sweep rate) from the curves at different scan rate of cells with or without GCN Li^+-modulating layer. The results show that the interfacial reaction kinetics could be accelerated assisted by this specially designed interfacial layer. e,f) Schematic illustrations of the general steps happening and energy barrier upon Li deposition over a bare anode surface (e) and the anode surface modified by the GCN Li^+-modulating layer (f).

solvent molecules in liquid electrolyte before deposition. Upon discharging, electrons transport to the anode via external circuit and solvated Li ions absorb to the anode surface followed by a desolvation process ahead of plating. In the absence of GCN Li^+-modulating layer, Li ions tend to accumulate at preferentially formed Li tips due to a comparatively shorter diffusion pathway and stronger electric field. The consequential uneven Li^+ distribution and transport hence result in severe dendrite growth. The stripping process also leads to considerable dead Li particles and large internal impedance (Figure 5c). Here the introduction of GCN nanosheets layer could prestabilized Li ions near the anode surface via transient Li—N bonds. Considering the ultrahigh electrochemical stability of GCN, the Li^+ distribution can be tailored steady upon cycling, contributing to a much denser and smoother deposition formation (Figure 5d). EIS measurements were also performed to reveal the evolutions of internal impedance with or without GCN Li^+ modulating layer (Figure S9, Supporting Information). It can be observed that all values of R_s, R_{sei}, and R_{ct} of cells cycled with GCN Li^+-modulating layer were markedly lower than that of pristine cells due to a well-maintained dense structure without dendrites and much dead Li particles upon cycling.

Finally, the electrochemical performance optimized by GCN Li^+-modulating was characterized. **Figure 6**a presents the voltage stability curves of bare and modified cells at a current density of 1 mA cm^{-2}. Smooth Li plating/stripping curves could

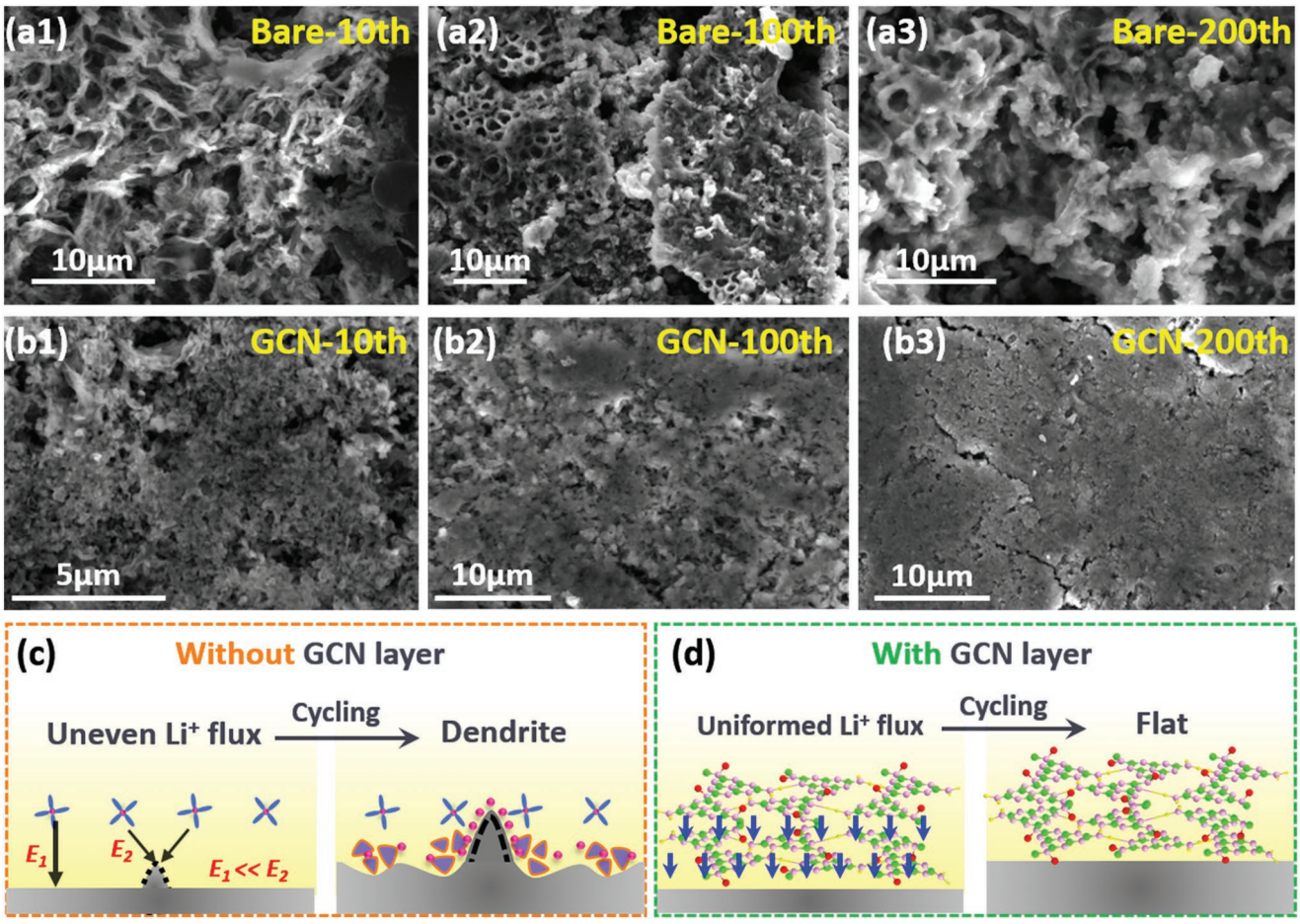

Figure 5. a,b) Morphology evolutions after specific plating/stripping cycles over a bare anode surface (a) and the anode surface modified by the GCN Li^+-modulating layer (b). c,d) Schematic illustrations of structural evolution upon deposition and corresponding mechanisms over the bare anode (c) and the modified anode (d).

be obtained with small voltage fluctuation in the presence of a GCN layer with a voltage hysteresis less than 110 mV for hundreds of cycles, indicating stable interfacial evolutions over the anode surface. In comparison, the voltage of bare cells shows a steep rise at the initial stage followed by a sudden drop at the end of 60 cycles due to possible short circuits. Similarly, the Coulombic efficiency (CE) of cell containing the GCN layer could maintain a value over 99% for 900 cycles (Figure 6b) while that of pristine cell diverges after 60 cycles. For bare anode, the deposition behaviors of Li ion are scarcely modulated and hence undergo a catastrophic structural evolutions which consumes amount of electrolyte and active Li source as indicated by aforementioned SEM images. On the contrary, the high and well-retained CE in GCN-modified cells are closely related to the smooth and dense deposition morphology with little dendrites and dead Li particles due to the formation of transient Li—N bonds and stabilized Li^+ distribution. The Li plating/stripping behaviors in the presence of GCN Li^+-modulating layer are further probed by the charge–discharge curves (Figure 6c,d). The initial CE increases with the help of GCN interfacial layer due to the tailored deposition behavior and reduced side reactions. At the end of the 60th cycle in bare cells, the voltage profile shakes, reflecting local short circuits in cell. Besides, it is surprising to detect that the discharge–charge curves in modified batteries become even steadier upon prolonged cycles without any voltage undulation. The comparison of cumulative capacity is presented in Figure 6e and this work clearly surpass most of existing papers. Here cumulative capacity is the summation of the capacity plated on each individual cycle prior to cell shorting or excessive impedance rise.[35] Rather than a mere comparison of cycle number, cumulative capacity is an overall indicator involving both deposition capacity and lifespan, which could better reflect the effectiveness of different tactics.[19,36–58] The introduction of GCN Li^+-modulating layer as well enables stable deposition at high current densities such as 2, 3, and 5 mA cm^{-2}. Besides, the modulating layer as well conduces to a uniform deposition exceeding 100 cycles with a high deposition capacity of 5 mAh cm^{-2}. The Coulombic efficiency data for a practical current and lithium plating capacity such as 3 mA cm^{-2} and 3 mAh cm^{-2} are also provided in Figure S10 (Supporting Information). The CE data of Li–Cu cells without g-C_3N_4 Li^+-modulating layer undergo severe fluctuations at around the 20th cycle. In contrast, Li–GCN–Cu cells could maintain a stable Coulombic efficiency and plating/stripping curves upon cycling. Such excellent performances are closely related to the prestabilized Li^+ distribution and decreased energy barrier

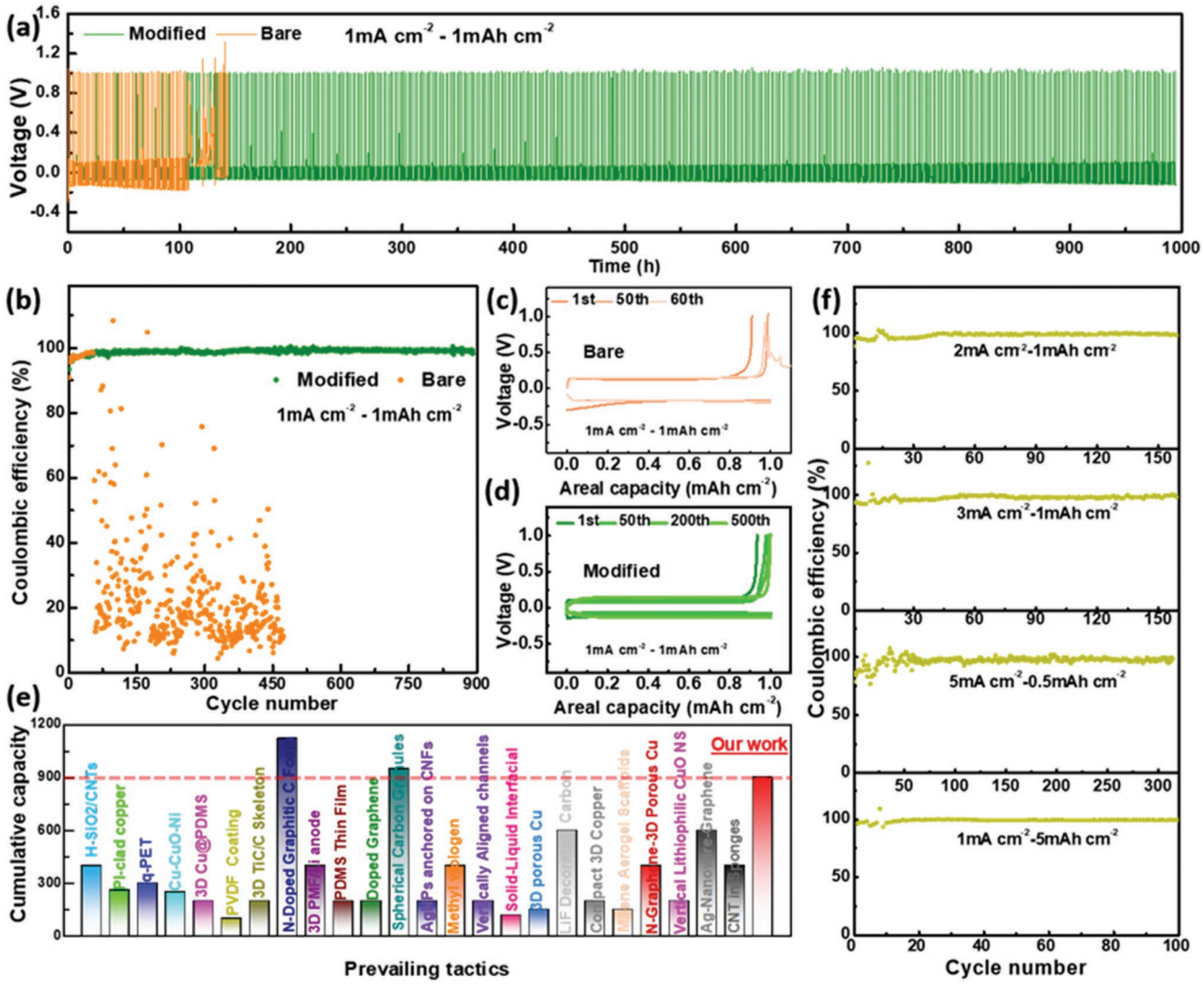

Figure 6. Electrochemical performance. a) Voltage–time curves, b) Coulombic efficiency, and c,d) corresponding discharge–charge profiles of cells using bare anode and the anode modified by the GCN Li^+-modulating layer. e) Comparison of cumulative capacities of existing papers. f) Coulombic efficiency of cells with the anode modified by the GCN Li^+-modulating layer, at high current densities and capacities.

that prohibits possible dendrite nucleation upon fast deposition and adequate Li ion flux to enable high-capacity deposition. Here Li–Cu cells is introduced majorly for characterizing the Coulombic efficiency. Additional electrochemical performance data for cells where the GCN layer is actually on the lithium-metal anode including Li–$LiFePO_4$ and Li–Li symmetric cells are presented in Figure S11 (Supporting Information). The results also clearly show the advantageous roles of the GCN layer in the electrochemical performances. To further confirm the important effects of N-species with g-C_3N_4, graphene oxide (GO) with similar structure to g-C_3N_4 but without any N atoms is also tried as the artificial interface layer by same autotransfer process (Figure S12, Supporting Information). It can be observed that the performance of graphene oxide–modified anode is much inferior to that of g-C_3N_4-modified anode. By these control experiments, it is safe to say that the large number of N atoms in the g-C_3N_4 layer help to render uniform lithium flux.

In summary, we successfully built an effective interfacial Li^+-modulating layer via a brand-new touching transfer technique. A thin g-C_3N_4 film was initially vacuum filtrated over a commercial separator in ambient air and then perfectly autotransferred to the Li surface merely by electrolyte wetting during normal cell assembly. Compared to traditional construction of interfacial layers, this autotransferable strategy shows little selectivity toward chemical reagents, atmospheric gases or drying conditions and thus dramatically minified the environmental requirements, costs, complexities and safety risks. And the rich N species render the formation of considerable transient Li—N bonds within the g-C_3N_4 film at the vicinity of the anode which conduces to the stabilization of Li^+ distribution to further prohibit dendrite growth for 900 cycles with a CE over 99% and endows reduced energy barrier and facilitated deposition kinetics as well as adequate Li^+ flux to enable stable deposition at higher current densities and capacities, surpassing most present researches. As a rule, our work

demonstrates a brand-new technique to build interfacial layer upon Li anode via a facile touching mode that dramatically water down the requirements on operation condition, costs and complexities. And this tactic vastly expands our choices of agents and material systems, shedding new light on fabricating some novel protective layers. Furthermore, the function mechanism of the N-species dominated GCN layer is revealed to be highly related to the formation of transient Li—N bonds which are capable to stabilize Li^+ distribution and lower the deposition energy barrier as well as facilitate the deposition kinetics in proximity to the anode upon Li plating/stripping.

Experimental Section

Synthesis: Bulk g-C_3N_4 power was prepared via heating certain amount of urea at 500 °C for 2 h at a ramp rate of 5 °C min^{-1}. The resultant yellow agglomerates were milled into powder in a mortar. Corresponding g-C_3N_4 nanosheets were fabricated by one-pot exfoliation of the above bulk g-C_3N_4 power bulk powder in isopropyl alcohol via an ultrasonication. In a typical fabrication, 30 mg of g-C_3N_4 powders were added to 25 mL flasks. 10 mL of isopropyl alcohol was added to the above flasks as dispersion solvent. The sealed flasks were sonicated for 10 h, and then the dispersions were centrifuged at 4000 rpm for 30 min to remove aggregates. Thus, the light-yellow exfoliated g-C_3N_4 nanosheets were obtained. To prepare the Li^+ modulating layer, g-C_3N_4 nanosheets/isopropyl alcohol supernatant of certain volume after centrifugation was then applied on a Celgard separator by a simple vacuum infiltration method. Finally, the GCN modulating layer was dried in a vacuum oven at 80 °C for 24 h. To characterize its Li^+ modulating properties of this g-C_3N_4 layer, the GCN layer is immersed into 1 M LiBr/isopropyl alcohol or LiBr/DI solution for 1 h and then taken out, washed with distilled water for 3 times and dried in a vacuum oven at 80 °C for 12 h for further characterization.

Characterizations: X-ray diffraction (PANalytical X'pert PRO-DY2198), X-ray photoelectron spectroscopy (AXIS-ULTRA DLD-600W), and Fourier transform infrared spectroscopy (Bruker VERTEX 70 FTIR spectrometer) were used to characterize the Li-modulating properties of the GCN layer. The morphology and microstructure of the as-prepared g-C_3N_4 nanosheets and layer were obtained using a scanning electron microscope (FEI Quanta650 FEG), a transmission electron microscope (FEI Tecnai JEL 2100) and an atomic force microscope (Dimension Icon, Bruker). The contact angle was measured via Kruss DSA 100.

Electrochemistry: Copper foil with or without a GCN Li^+ modulating layer was assembled against bare Li electrodes with CR2032-type coin cells to test the Coulombic efficiency. The coin cells were assembled in argon-filled glove box, which were composed of copper foil, GCN layer, Celgard separators, bare Li electrodes (reference/counterelectrode) and the electrolyte (1 M LiTFSI dissolved in DOL/DME with 5% mass ratio $LiNO_3$). The batteries were first cycled between 0 and 1 V at 50 μA for five cycles to stabilize the surface SEI. The measurement was performed at current densities of 1, 2, 3, and 5 mA cm^{-2} at room temperature. The Coulombic efficiency of cycling was calculated based on the ratio of discharge and charge capacity. Galvanostatic charge–discharge experiments were carried out with a LAND battery testing system. Cyclic voltammetry (CV) tests were carried out using the CHI 760E electrochemical workstation. The electrochemical impedance spectroscopy tests were conducted on the Solartron Electrochemical Interface SI 1287 and SI 1260 from 0.01 to 100 000 Hz with the amplitude of 5 mV.

Supporting Information

Supporting Information is available from the Wiley Online Library or from the author.

Acknowledgements

The authors would like to acknowledge the support from the National Basic Research Program of China (2015CB932600), National Natural Science Foundation of China (21571073 and 51772115), Hubei Provincial Natural Science Foundation of China (2016CFA031), and the Fundamental Research Funds for the Central University (2017KFKJXX007 and 2015ZDTD038). The authors also thank the Analytical and Testing Center of HUST for the measurements.

Conflict of Interest

The authors declare no conflict of interest.

Keywords

interfacial layers, lithium anodes, lithium dendrites, lithium-metal batteries, stable deposition

Received: January 15, 2019
Revised: April 7, 2019
Published online: May 16, 2019

[1] P. G. Bruce, S. A. Freunberger, L. J. Hardwick, J. M. Tarascon, *Nat. Mater.* **2012**, *11*, 19.
[2] L. Grande, E. Paillard, J. Hassoun, J. B. Park, Y. J. Lee, Y. K. Sun, S. Passerini, B. Scrosati, *Adv. Mater.* **2015**, *27*, 784.
[3] X. Chen, T.-Z. Hou, B. Li, C. Yan, L. Zhu, C. Guan, X.-B. Cheng, H.-J. Peng, J.-Q. Huang, Q. Zhang, *Energy Storage Mater.* **2017**, *8*, 194.
[4] Y. Zhang, Y. Zhong, Q. Shi, S. Liang, H. Wang, *J. Phys. Chem. C* **2018**, *122*, 21462.
[5] Y. Guo, H. Li, T. Zhai, *Adv. Mater.* **2017**, *29*, 1700007.
[6] D. Lin, Y. Liu, Y. Cui, *Nat. Nanotechnol.* **2017**, *12*, 194.
[7] X.-B. Cheng, R. Zhang, C.-Z. Zhao, Q. Zhang, *Chem. Rev.* **2017**, *117*, 10403.
[8] V. Augustyn, M. T. McDowell, A. Vojvodic, *Joule* **2018**, *2*, 2189.
[9] J.-i. Yamaki, S.-i. Tobishima, K. Hayashi, S. Keiichi, Y. Nemoto, M. Arakawa, *J. Power Sources* **1998**, *74*, 219.
[10] N.-W. Li, Y. Shi, Y.-X. Yin, X.-X. Zeng, J.-Y. Li, C.-J. Li, L.-J. Wan, R. Wen, Y.-G. Guo, *Angew. Chem., Int. Ed.* **2018**, *57*, 1505.
[11] X. Liang, Q. Pang, I. R. Kochetkov, M. S. Sempere, H. Huang, X. Sun, L. F. Nazar, *Nat. Energy* **2017**, *2*, 17119.
[12] X. Han, Y. Gong, K. K. Fu, X. He, G. T. Hitz, J. Dai, A. Pearse, B. Liu, H. Wang, G. Rubloff, Y. Mo, V. Thangadurai, E. D. Wachsman, L. Hu, *Nat. Mater.* **2017**, *16*, 572.
[13] Y. Liu, C. Li, B. Li, H. Song, Z. Cheng, M. Chen, P. He, H. Zhou, *Adv. Energy Mater.* **2018**, *8*, 1702374.
[14] J. Lopez, A. Pei, J. Y. Oh, G.-J. N. Wang, Y. Cui, Z. Bao, *J. Am. Chem. Soc.* **2018**, *140*, 11735.
[15] Y. Liu, Y.-K. Tzeng, D. Lin, A. Pei, H. Lu, N. A. Melosh, Z.-X. Shen, S. Chu, Y. Cui, *Joule* **2018**, *2*, 1595.
[16] X. B. Cheng, T. Z. Hou, R. Zhang, H. J. Peng, C. Z. Zhao, J. Q. Huang, Q. Zhang, *Adv. Mater.* **2016**, *28*, 2888.
[17] Z. Liang, G. Zheng, C. Liu, N. Liu, W. Li, K. Yan, H. Yao, P. C. Hsu, S. Chu, Y. Cui, *Nano Lett.* **2015**, *15*, 2910.
[18] M. H. Ryou, D. J. Lee, J. N. Lee, Y. M. Lee, J. K. Park, J. W. Choi, *Adv. Energy Mater.* **2012**, *2*, 645.
[19] R. Zhang, X. R. Chen, X. Chen, X. B. Cheng, X. Q. Zhang, C. Yan, Q. Zhang, *Angew. Chem., Int. Ed.* **2017**, *56*, 7764.

[20] E. Cha, M. D. Patel, J. Park, J. Hwang, V. Prasad, K. Cho, W. Choi, *Nat. Nanotechnol.* **2018**, *13*, 337.
[21] Y. Li, Y. Li, Y. Sun, B. Butz, K. Yan, A. L. Koh, J. Zhao, A. Pei, Y. Cui, *Nano Lett.* **2017**, *17*, 5171.
[22] Z. Lu, Q. Liang, B. Wang, Y. Tao, Y. Zhao, W. Lv, D. Liu, C. Zhang, Z. Weng, J. Liang, H. Li, Q.-H. Yang, *Adv. Energy Mater.* **2019**, *9*, 1803186.
[23] J. Hu, J. Tian, C. Li, *ACS Appl. Mater. Interfaces* **2017**, *9*, 11615.
[24] Y. Shi, S. Jiang, K. Zhou, C. Bao, B. Yu, X. Qian, B. Wang, N. Hong, P. Wen, Z. Gui, Y. Hu, R. K. Yuen, *ACS Appl. Mater. Interfaces* **2014**, *6*, 429.
[25] Y. Guo, Y. Wei, H. Li, T. Zhai, *Small* **2017**, *13*, 1701649.
[26] R. Mukherjee, A. V. Thomas, D. Datta, E. Singh, J. Li, O. Eksik, V. B. Shenoy, N. Koratkar, *Nat. Commun.* **2014**, *5*, 3710.
[27] Y. Kang, Y. Yang, L.-C. Yin, X. Kang, G. Liu, H.-M. Cheng, *Adv. Mater.* **2015**, *27*, 4572.
[28] P. Niu, L.-C. Yin, Y.-Q. Yang, G. Liu, H.-M. Cheng, *Adv. Mater.* **2014**, *26*, 8046.
[29] K. Yan, Z. Lu, H.-W. Lee, F. Xiong, P.-C. Hsu, Y. Li, J. Zhao, S. Chu, Y. Cui, *Nat. Energy* **2016**, *1*, 16010.
[30] J. M. Whiteley, S. Hafner, S. S. Han, S. C. Kim, K. H. Oh, S.-H. Lee, *Adv. Energy Mater.* **2016**, *6*, 1600495.
[31] N. Nakayama, T. Nozawa, Y. Iriyama, T. Abe, Z. Ogumi, K. Kikuchi, *J. Power Sources* **2007**, *174*, 695.
[32] D. Lin, Y. Liu, W. Chen, G. Zhou, K. Liu, B. Dunn, Y. Cui, *Nano Lett.* **2017**, *17*, 3731.
[33] P. Simon, Y. Gogotsi, B. Dunn, *Science* **2014**, *343*, 1210.
[34] V. Augustyn, J. Come, M. A. Lowe, J. W. Kim, P. L. Taberna, S. H. Tolbert, H. D. Abruna, P. Simon, B. Dunn, *Nat. Mater.* **2013**, *12*, 518.
[35] P. Albertus, S. Babinec, S. Litzelman, A. Newman, *Nat. Energy* **2018**, *3*, 16.
[36] W. Zhang, H. L. Zhuang, L. Fan, L. Gao, Y. Lu, *Sci. Adv.* **2018**, *4*, eaar4410.
[37] X. Wang, W. Zeng, L. Hong, W. Xu, H. Yang, F. Wang, H. Duan, M. Tang, H. Jiang, *Nat. Energy* **2018**, *3*, 227.
[38] P. Zou, Y. Wang, S. W. Chiang, X. Wang, F. Kang, C. Yang, *Nat. Commun.* **2018**, *9*, 464.
[39] T.-T. Zuo, Y.-X. Yin, S.-H. Wang, P.-F. Wang, X. Yang, J. Liu, C.-P. Yang, Y.-G. Guo, *Nano Lett.* **2018**, *18*, 297.
[40] H. Ye, S. Xin, Y.-X. Yin, J.-Y. Li, Y.-G. Guo, L.-J. Wan, *J. Am. Chem. Soc.* **2017**, *139*, 5916.
[41] K. Liu, A. Pei, H. R. Lee, B. Kong, N. Liu, D. Lin, Y. Liu, C. Liu, P.-c. Hsu, Z. Bao, Y. Cui, *J. Am. Chem. Soc.* **2017**, *139*, 4815.
[42] H. Wu, Y. Cao, L. Geng, C. Wang, *Chem. Mater.* **2017**, *29*, 3572.
[43] S. Wu, Z. Zhang, M. Lan, S. Yang, J. Cheng, J. Cai, J. Shen, Y. Zhu, K. Zhang, W. Zhang, *Adv. Mater.* **2018**, *30*, 1705830.
[44] B. Zhu, Y. Jin, X. Hu, Q. Zheng, S. Zhang, Q. Wang, J. Zhu, *Adv. Mater.* **2017**, *29*, 1603755.
[45] C. Yang, Y. Yao, S. He, H. Xie, E. Hitz, L. Hu, *Adv. Mater.* **2017**, *29*, 1702714.
[46] S.-H. Wang, Y.-X. Yin, T.-T. Zuo, W. Dong, J.-Y. Li, J.-L. Shi, C.-H. Zhang, N.-W. Li, C.-J. Li, Y.-G. Guo, *Adv. Mater.* **2017**, *29*, 1703729.
[47] L. Liu, Y.-X. Yin, J.-Y. Li, S.-H. Wang, Y.-G. Guo, L.-J. Wan, *Adv. Mater.* **2018**, *30*, 1706216.
[48] Q. Li, S. Zhu, Y. Lu, *Adv. Funct. Mater.* **2017**, *27*, 1606422.
[49] J. Luo, C.-C. Fang, N.-L. Wu, *Adv. Energy Mater.* **2018**, *8*, 1701482.
[50] S. Liu, X. Xia, Y. Zhong, S. Deng, Z. Yao, L. Zhang, X.-B. Cheng, X. Wang, Q. Zhang, J. Tu, *Adv. Energy Mater.* **2018**, *8*, 1702322.
[51] L. Fan, H. L. Zhuang, W. Zhang, Y. Fu, Z. Liao, Y. Lu, *Adv. Energy Mater.* **2018**, *8*, 1703360.
[52] J. Xie, J. Ye, F. Pan, X. Sun, K. Ni, H. Yuan, X. Wang, N. Shu, C. Chen, Y. Zhu, *Adv. Mater.* **2019**, *31*, e1805654.
[53] M. Wang, Z. Peng, W. Luo, F. Ren, Z. Li, Q. Zhang, H. He, C. Ouyang, D. Wang, *Adv. Energy Mater.* **2019**, *9*, 1802912.
[54] H. Zhao, D. Lei, Y.-B. He, Y. Yuan, Q. Yun, B. Ni, W. Lv, B. Li, Q.-H. Yang, F. Kang, J. Lu, *Adv. Energy Mater.* **2018**, *8*, 1800266.
[55] X. Zhang, R. Lv, A. Wang, W. Guo, X. Liu, J. Luo, *Angew. Chem., Int. Ed.* **2018**, *57*, 15028.
[56] R. Zhang, S. Wen, N. Wang, K. Qin, E. Liu, C. Shi, N. Zhao, *Adv. Energy Mater.* **2018**, *8*, 1800914.
[57] C. Zhang, W. Lv, G. Zhou, Z. Huang, Y. Zhang, R. Lyu, H. Wu, Q. Yun, F. Kang, Q.-H. Yang, *Adv. Energy Mater.* **2018**, *8*, 1703404.
[58] P. Xue, S. Liu, X. Shi, C. Sun, C. Lai, Y. Zhou, D. Sui, Y. Chen, J. Liang, *Adv. Mater.* **2018**, *30*, 1804165.

